Controlled Hydrothermal Synthesis of Bismuth Oxybromides and Their Visible-Light-Responsive Photocatalytic Properties

Yu-Rou Jiang(蔣語柔), Hong Lin Chen (陳泓霖), Yen-Ju Chen (陳彥如), Chiing-Chang Chen (陳錦章)*

Department of Science Application and Dissemination, National Taichung University of Education
*Email: ccchen@mail.ntcu.edu.tw

Abstract

Ternary bismuth oxybromides have been synthesized using autoclave hydrothermal methods. In the preparation procedure, Bi $(NO_3)_3 \cdot 5H_2O$ is dissolved in HNO_3, NaOH aqueous solution is added to adjust the pH value, and then KBr aqueous solution is added to the suspension. The composition and morphologies of bismuth oxybromides can be controlled by adjusting certain growth parameters, including reaction pH, time, and temperature. The products are characterized by XRD, FE-SEM-EDS, HR-XPS, FT-IR, and DRS. We demonstrate that Bi_5O_7Br, Bi_3O_4Br, $Bi_{24}O_{31}Br_{10}$, $Bi_4O_5Br_2$, and BiOBr can be selectively prepared through a facile solution-based hydrothermal method. UV-Vis spectra show bismuth oxybromide materials to be indirect semiconductors with an optical bandgap of 2.22-2.76 eV. Crystal violet (CV) has been reported to endanger human health. Therefore, treating wastewater is necessary. Photocatalytic efficiencies of powder suspensions were evaluated by measuring the CV concentration. This is the first study to show the superior activities of Bi_5O_7Br, Bi_3O_4Br, $Bi_{24}O_{31}Br_{10}$, and $Bi_4O_5Br_2$ as a promising visible-light- responsive photocatalyst. Finally, the intermediates of the process are separated, identified, and characterized by HPLC-PDA-ESI-MS to conjecture the *N*-de-methylation, hydroxylation, and cleavage of the conjugated chromophore structure degradation of CV dye.

Keywords: Bismuth oxybromide, Autoclave hydrothermal, Visible-light-responsive photocatalyst

NSC Project no.: NSC 99-2113-M-142-001-MY2

1 Introduction

Heterogeneous photocatalysis for environmental remediation and solar energy conversion has aroused extensive interest in the past decade. For the practical application of photocatalysis, an environmentally sturdy and inexpensive photocatalyst is an important component [1]. Among the various photocatalytic materials, nano-scaled TiO_2 is studied most, however, it can only be activated by irradiation under UV, which contains less than 5% of the solar spectrum [2]. To utilize visible light (43% energy in solar spectrum) and harvest solar energy efficiently, intensive efforts have attempted to develop visible-light-responsive photocatalysts, such as metal/nonmetal doped TiO_2 [3], inorganic bismuth compounds (Bi_2WO_6 [4], Bi_2MoO_6 [5] and $BiVO_4$ [6]), and ferrites [7]. Although most photocatalysts show markedly visible-light-responsive activity, their stabilities, the relationship between structure and photocatalytic reactivity, and photocatalysis mechanisms remain uncertain [8]. Therefore, synthesizing novel visible- light-responsive photocatalysts and exploring their photocatalysis performance are of great interest and potential award [9].

Bismuth oxyhalides, BiOX (X = Cl, Br, I), belong to the family of main group multi-component metal oxyhalides V–VI–VII, an important class of ternary compounds, which have recently induced great interest because of their unique and excellent optical, electrical, magnetic, and photoluminescence properties and because of their potential photocatalytic abilities [10]. Among the bismuth oxyhalides, bismuth oxybromides have received remarkable attention in recent years because of their stability, suitable band gaps, and relatively superior

photocatalytic abilities. BiOBr flakes showed superior photocatalytic abilities than P25 TiO_2 in degrading dyes under visible light (>400 nm) illumination [11]. The Fang group synthesized BiOBr by hydrothermal methods, which exhibited excellent photocatalytic efficiency and good stability during microcystin-LR photodegradation under visible light irradiation [12]. The other bismuth oxybromide photocatalyst may be an efficient functional material for the environmental purification of organic pollutants in aqueous solution. To the best of our knowledge, photocatalytic degradation of organic pollutants by Bi_5O_7Br, Bi_3O_4Br, $Bi_{24}O_{31}Br_{10}$, and $Bi_4O_5Br_2$ have not been documented in the literature. This study synthesized Bi_5O_7Br, Bi_3O_4Br, $Bi_{24}O_{31}Br_{10}$, and $Bi_4O_5Br_2$ and studied their photocatalytic ability for removing CV in aqueous solutions under visible-light irradiation. The other bismuth oxybromide photocatalysts with high photocatalytic performance were prepared by controlling synthesis conditions, and the removal efficiency, principal reaction products, and CV degradation pathway using the prepared bismuth oxybromides were also explored. Li et al. recently reported a facile, hydrothermal synthetic pathway for preparing single-crystalline nano-belts of bismuth oxyhalides [13]. Our further studies showed that, by manipulating appropriate reaction parameters such as pH, temperature, and time, ternary bismuth oxybromides with different compositions could be selectively synthesized. In this paper, a systematic study has been performed to investigate the controlled synthesis of bismuth oxybromides by adjusting selected growth parameters, and a suitable mechanism has been proposed for their formation.

2 Experimental

2.1 Materials

The purchased Bi $(NO_3)_3$•$5H_2O$, CV dye (TCI), and KBr (Katayama) were obtained and used without any further purification. Reagent-grade nitric acid, sodium hydroxide, ammonium acetate, and HPLC-grade methanol were obtained from Merck. The de-ionized water used in this study was purified with a Milli-Q water ion-exchange system (Millipore Co.) for a resistivity of 1.8×10^7 Ω-cm.

2.2 Synthesis of bismuth oxybromide

5 mmol of Bi $(NO_3)_3$•$5H_2O$ were first mixed in a 100 mL flask, followed by adding 5 mL of 4M HNO_3. With continuous stirring, 2 M of NaOH were added dropwise to adjust the pH value to 1–14 and when a white precipitate was formed, then 2 mL of KBr were also added dropwise. The solution was then stirred vigorously for 30 min and transferred into a 30 mL Teflon-lined autoclave, which was heated to 60–280 ^oC for 12, 24, and 36 h and then naturally cooled to room temperature. After the reaction was completed, the resulting solid product was collected by filtration, then washed with deionized water and methanol to remove any possible ionic species in the product, and then dried at 60 ^oC overnight. The samples are listed in Table 1.

Table 1: Bismuth oxybromides obtained under different reaction conditions.

T(°) t(h) / pH	110°C/ 12h	160°C/ 12h	210°C/ 12h	260°C/ 12h
1	BB- 1-110-12	BB- 1-160-12	BB- 1-210-12	BB- 1-260-12
2	BB- 2-110-12	BB- 2-160-12	BB- 2-210-12	BB- 2-260-12
3	BB- 3-110-12	BB- 3-160-12	BB- 3-210-12	BB -3-260-12
4	BB -4-110-12	BB- 4-160-12	BB- 4-210-12	BB- 4-260-12
5	BB- 5-110-12	BB- 5-160-12	BB- 5-210-12	BB- 5-260-12
6	BB -6-110-12	BB- 6-160-12	BB- 6-210-12	BB- 6-260-12
7	BB- 7-110-12	BB- 7-160-12	BB- 7-210-12	BB- 7-260-12
8	BB- 8-110-12	BB- 8-160-12	BB- 8-210-12	BB- 8-260-12
9	BB -9-110-12	BB- 9-160-12	BB- 9-210-12	BB- 9-260-12
10	BB- 10-110-12	BB- 10-160-12	BB- 10-210-12	BB- 10-260-12
11	BB- 11-110-12	BB- 11-160-12	BB- 11-210-12	BB- 11-260-12
11.5	BB- 11.5-110-12	BB- 11.5-160-12	BB- 11.5-210-12	BB- 11.5-260-12
12	BB- 12-110-12	BB- 12-160-12	BB- 12-210-12	BB- 12-260-12
13	B-B 13-110-12	BB -13-160-12	BB- 13-210-12	BB- 13-260-12
14	BB- 14-110-12	BB- 14-160-12	BB -14-210-12	BB- 14-260-12

2.3 Characterization

The precipitates were further characterized. Powder X-ray diffraction (XRD) was performed on a MAC Science, MXP18 X-ray diffractometer with Cu Kα radiation, and operated at 40 kV and 80 mA. FE-SEM-EDS measurements were carried out with a field-emission microscope (JEOL JSM-7401F) at an acceleration voltage of 15 kV and an HRXPS measurement was conducted with ULVAC-PHI XPS. The Al Kα radiation was generated with a voltage of 15 kV. Absorption measurements were

conducted using a Shimadzu UV-2100S spectrophotometer. The HPLC-PDA-ESI-MS system consisted of a Waters 1525 binary pump, a 2998 photodiode array detector, and a 717 plus autosampler.

2.4 Photocatalytic reaction

Photocatalytic activities of bismuth oxybromides were studied by degrading CV under visible light irradiation of a 20 watt lamp. An average irradiation intensity of 5.2 W/m^2 was maintained throughout the experiments and was measured by internal radiometer. Aqueous dispensions of CV (100 mL, 10 ppm) and the given amount of catalyst powder were placed in a Pyrex flask. The pH value of the dispension was adjusted by adding either NaOH or HNO_3 solutions. Before irradiation, the dispensions were magnetically stirred in the dark for 30 min to reach an adsorption/desorption equilibrium between the dye and the catalyst surface under ambient air-equilibrated conditions. At the given irradiation time intervals, 5 mL of aliquot were collected and centrifuged to remove the catalyst. The supernatant was analyzed by HPLC-ESI-MS after readjusting the chromatographic conditions to make the mobile phase compatible with the working conditions of the mass spectrometer.

3 Results and Discussion

3.1 Characterizations of as-prepared powders

3.1.1 XRD analysis

The X-ray diffraction data of bismuth oxybromide samples prepared with different hydrothermal parameters are shown in Figure1(a)-(c). All the bismuth oxybromide samples synthesized using the hydrothermal method described at different temperatures and pH are the Bi_5O_7Br (JCPDS 38-0493), Bi_3O_4Br (JCPDS 84-0793), $Bi_{24}O_{31}Br_{10}$ (JCPDS 75-0888), and $Bi_4O_5Br_2$ (JCPDS 37-0669) phase. Figure 1(a) shows X-ray diffraction data for bismuth oxybromide samples prepared at pH=1-14 for 110°C and 12 h, respectively. The pH of a reaction is generally accepted to have great influence on determining the composition and morphologies of the final products [13]. Control experiments have been conducted to investigate the influence of pH on the reaction. In our experiment, pH plays a key role in controlling the composition and anisotropic growth of crystals. The results are listed in Fig. 1(a). We prepared BiOBr at pH 1–7; $Bi_4O_5Br_2$ at pH 2–11.5; $Bi_{24}O_{31}Br_{10}$ at pH 7-9; Bi_3O_4Br at pH 3–13; whereas, Bi_2O_3 microstructures were prepared under more basic (pH>14) conditions. The possible processes for the formation of bismuth oxybromides are described as follows [Eqs. (1) – (6)]:

$$Bi^{3+} + 3OH^- \rightarrow Bi(OH)_{3(s)} \quad (1)$$

$$2Bi(OH)_{3(s)} + Br^- \rightarrow BiOBr_{(s)} + H_2O + OH^- \quad (2)$$

$$4BiOBr_{(s)} + 2OH^- \rightarrow Bi_4O_5Br_{2(s)} + 2Br^- + H_2O \quad (3)$$

$$6Bi_4O_5Br_{2(s)} + 2OH^- \rightarrow Bi_{24}O_{31}Br_{10(s)} + 2Br^- + H_2O \quad (4)$$

$$Bi_{24}O_{31}Br_{10(s)} + 2OH^- \rightarrow 8Bi_3O_4Br_{(s)} + 2Br^- + H_2O \quad (5)$$

$$5Bi_3O_4Br_{(s)} + 2OH^- \rightarrow 3Bi_5O_7Br_{(s)} + 2Br^- + H_2O \quad (6)$$

$$12Bi_5O_7Br_{(s)} + 2OH^- \rightarrow 5Bi_{12}O_{17}Br_{2\,(s)} + 2Br^- + H_2O \quad (7)$$

$$Bi_{12}O_{17}Br_{2\,(s)} + 2OH^- \rightarrow 6Bi_2O_{3(s)} + 2Br^- + H_2O \quad (8)$$

These equations show that BiOBr was formed at the beginning of the reaction, then OH^- gradually substituted Br^- in the basic conditions, which resulted in the reduced content of Br^- in the products. Increasing the pH gradually obtained $Bi_4O_5Br_2$, $Bi_{24}O_{31}Br_{10}$, Bi_3O_4Br, and Bi_5O_7Br. The higher the pH value, the lower the Br^- content in the products, until the content of Br^- in the products was fully replaced by OH^-, finally resulting in the formation of Bi_2O_3 under strong basic conditions. However, BiOBr is the exclusive product at pH 1. A competitive relationship typically exists between the OH^- and Br^- ions in basic solution. By controlling the pH of the reaction, different compositions of bismuth oxybromide were obtained.

Figure 1(b) shows X-ray diffraction data for bismuth oxybromide samples prepared at 60, 85, 110, 160, 230, and 280 °C for 12 h under pH=11.5, respectively. We prepared Bi $(OH)_3$ at 60°C; $Bi_4O_5Br_2$ and Bi_3O_4Br at 85 and 110°C; whereas, Bi_5O_7Br were prepared at higher temperature (>160°C) conditions. Figure 1(c) shows no observed phase changes regardless of the variation of hydrothermal time.

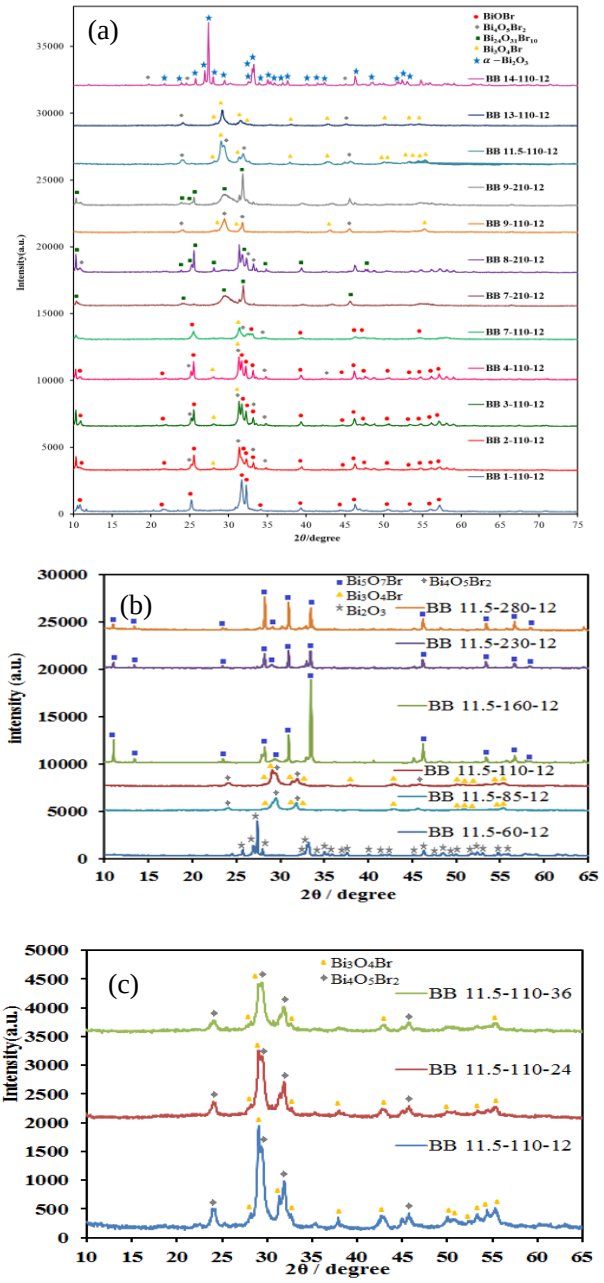

Figure 1: XRD patterns of as-prepared powders under different (a) pH value, (b) reaction temperature, and (c) reaction times.

3.1.2 SEM-EDS analysis

Bismuth oxybromides were prepared with Bi $(NO_3)_3$•$5H_2O$ and KBr by the hydrothermal method at 110 ^oC for pH 4, 7, 9, and 11.5. The surface morphology of the photocatalysts was examined by FE-SEM-EDS (**Figure 2**). These samples displayed irregular nanoplates and nanosheet shapes with a lateral size of several micrometers and a thickness between 5 and 10 nm. Sample BB-9-110-12 exhibits a plate-like irregular shape with a lateral size of several micrometers.

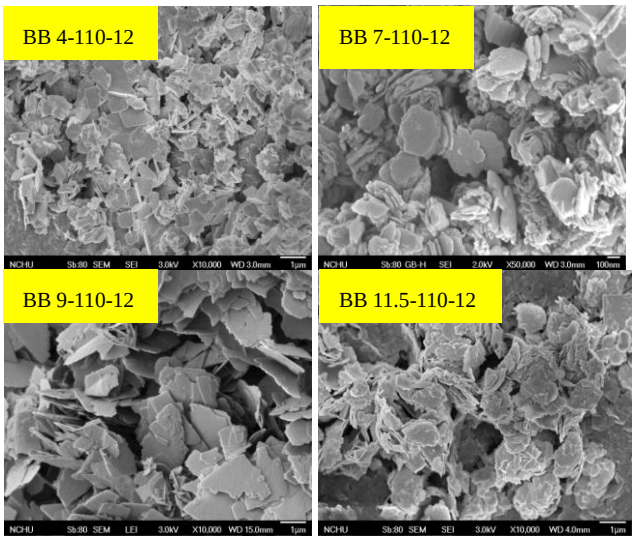

Figure 2: SEM images and EDS of bismuth oxybromide nanosheets prepared by the hydrothermal autoclave method at 110 ˚C, 12 h; for pH= 4 (a), 7 (b), 9 (c), and 11.5 (d).

3.1.3 XPS analysis

XPS is employed to examine the purity of the prepared bismuth oxybromide products, and the spectra are shown in **Figure 3**. The characteristic binding energy value of 157.9 eV for Bi $4f_{7/2}$ (**Figure 3 (b)**) revealed a trivalent oxidation state for bismuth. An additional spin–orbit doublet with binding energy of 155.5 eV for Bi $4f_{7/2}$ was also observed in all samples, suggesting that certain parts of bismuth existed in the (+3-x) valence state. This indicated that the trivalent bismuth partially reduced to the lower valence state by the hydrothermal autoclave method. A similar chemical shift of approximately 2.4-2.6 eV for Bi $4f_{7/2}$ was also observed by Jovalekic et al. [15]. They concluded that Bi $^{(+3-x)}$ formal oxidation state could most probably be attributed to the substoichiometric forms of Bi within the Bi_2O_2 layer, and formation of the low oxidation state resulted in oxygen vacancy in the crystal lattice. However, we assumed that Bi $^{(+3-x)}$ formal oxidation state could most likely be attributed to the substoichiometric forms of Bi at the outer site of the particles, and formation of the low oxidation state resulted in oxygen vacancy in the crystal surface. The binding energy of 68.6 eV and 67.8 eV were referred to the Br $3d_{5/2}$ and $3d_{3/2}$ respectively which can be assigned to the Br at the monovalent oxidation state. **Figure 4** shows the total survey spectra of the Bi 4f, Br 3d, O1s XPS of the four bismuth oxybromide samples.

According to the XPS spectra, observation of the transition peaks involving the Bi 4f, Br 3d, O 1s, and C 1s orbitals reveals that the catalysts are constituted by elements of C, O, Bi, and Br. In the BB-11.5-60-12 sample, only two strong peaks centered at 163.4 and 158.1 eV can be attributed to the Bi $4f_{5/2}$ and Bi $4f_{7/2}$, demonstrating that the main chemical states of the bismuth element in the samples were trivalent. The XPS result reveals that the synthesized BB-11.5-60-12 sample is pure in phase, which is consistent with the previous result by XRD analysis.

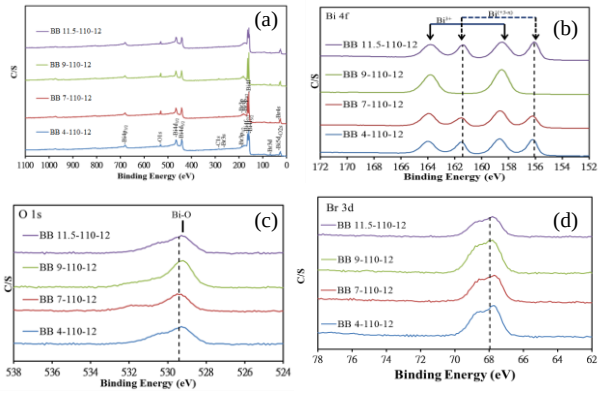

Figure 3. High-resolution XPS spectra of the bismuth oxybromide prepared by the hydrothermal autoclave method at 110 ˚C, 12 h, pH= 4, 7, 9, and 11.5. (a) Total survey; (b) Bi 4f; (c) O 1s; (d) Br 3d.

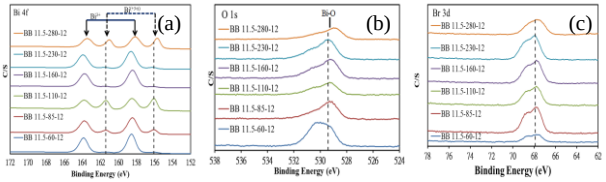

Figure 4. High-resolution XPS spectra of the bismuth oxybromide prepared by the hydrothermal autoclave method at pH 11.5, 12 h, temperature = 60, 85, 110, 160, 230, and 280 ˚C. (a) Total survey; (b) Bi 4f; (c) O 1s; (d) Br 3d.

3.1.4 UV–vis diffuse reflectance spectroscopy

The UV – vis adsorption spectra of synthesized catalysts are shown in **Figure 5**. Their corresponding band gap energies were calculated, which are close to 2.22-2.76 eV. Compared to P25, bismuth oxybromides exhibit pronounced light absorbance abilities at λ > 400 nm, suggesting their potential photocatalytic activity under visible light. The steep shape and strong absorption in the visible region ascribe the visible light absorption to the intrinsic band gap transition between the valence band and the conduction band, rather than the transition from the impurity levels [16]. The difference of band gap energy in the prepared bismuth oxybromide can be ascribed to their individual composition with various characteristics.

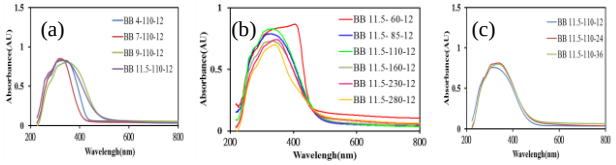

Figure 5: UV-vis absorption spectra of the prepared bismuth oxybromide catalysts. (a) pH = 4-11.5; (b) Temp = 60-280˚C; (c) Time = 12-36 h.

3.2 Photocatalytic Activity Evaluation

Photocatalytic performance of the bismuth oxybromide catalysts was evaluated by degrading CV under visible light or UV irradiation with 0.5 g/L of catalyst added. The degradation efficiencies as a function of reaction time are illustrated in **Figure 6**. In the absence of catalysts, CV could not be degraded under visible or UV light irradiation. The removal efficiency was enhanced significantly in the presence of bismuth oxybromide catalysts. After 48 h irradiation, bismuth oxybromide showed superior photocatalytic performance, with CV removal efficiency up to 99.9%. The superior photocatalytic ability of bismuth oxybromide may be ascribed to its efficient utilization of visible light and the high separation efficiency of the electron-hole pairs with its hieratical structure.

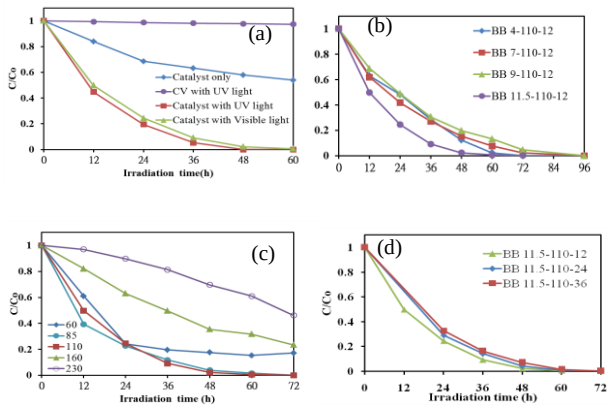

Figure 6: Photocatalytic degradation of CV by the resulting bismuth oxybromide catalysts and the control experiments under simulated visible light irradiation. (a) pH =4-11.5; (b) Temp=60-280˚C; (c) Time=12-36 h.

4 Conclusion

Bismuth oxybromide was synthesized by a facile hydrothermal method with Bi $(NO_3)_3$ and KBr as the Bi and Br source. The prepared bismuth oxybromide catalysts were of different phases, which removed nearly 100% of CV from the solution after 48 h under visible light irradiation, and the high photoactivity can be attributed to their relatively efficient utilization of visible light. Both removal efficiencies and kinetic analysis demonstrated the superior photocatalytic ability of bismuth oxybromide.

Acknowledgments

This research was supported by the National Science Council of the Republic of China.

References

[1] S. Malato, P. Fernández-Ibá˜nez, M.I. Maldonado, J. Blanco, W. Gernjak. "Decontamination and disinfection of water by solar photocatalysis: recent overview and trends" , *Catal. Today*, **147**, pp.1–59, 2009.

[2] M. A. Shannon, P. W. Bohn, M. Elimelech, J. G. Georgiadis, B. J. Marinas, A. M. Mayes. "Science and technology for water purification in the coming decades", *Nature*, **452**, p.p. 301–310, 2008.

[3] S. U. M. Khan, M. Al-Shahry, W. B. Ingler. "Efficient photochemical water splitting by a chemically modified n-TiO_2", *Science*, **297**, pp. 2243–2245, 2002.

[4] Y. H. B. Liao, J. X. Wang, J. S. Lin, W. H. Chung, W. Y. Lin, C. C. Chen. "Synthesis photocatalytic activities and degradation mechanism of Bi_2WO_6 toward crystal violet dye", *Catal. Today*, **174,** pp. 148-159, 2011.

[5] J. Ren, W. Wang, M. Shang, S. Sun and E. Gao. " Heterostructured Bismuth Molybdate Composite: Preparation and Improved Photocatalytic Activity under Visible-Light Irradiation", *ACS Appl. Mater. Interfaces*, **3**, pp. 2529–2533, 2011.

[6] D. Wang, R. Li, J. Zhu, J. Shi, J. Han, X. Zong and C. Li. "Photocatalytic Water Oxidation on $BiVO_4$ with the Electrocatalyst as an Oxidation Cocatalyst: Essential Relations between Electrocatalyst and Photocatalyst", *J. Phys. Chem. C*, **116**, pp. 5082–5089, 2012.

[7] E. Casbeer, V.K. Sharma and X.-Z. Li. "Synthesis and photocatalytic activity of ferrites under visible light: A review", *Sep. Purif. Technol.*, **87**, pp. 1-14, 2012.

[8] A. Kudo, K. Omori, H. Kato. "A Novel Aqueous Process for Preparation of Crystal Form-Controlled and Highly Crystalline $BiVO_4$ Powder from Layered Vanadates at Room Temperature and Its Photocatalytic and Photophysical Properties", *J. Am. Chem. Soc.*, **121**, pp. 11459–11467, 1999.

[9] J. Xu, W. Meng, Y. Zhang, L. Li, C. Guo. "Photocatalytic degradation of tetrabromobisphenol A by mesoporous BiOBr: Efficacy, products and pathway", *Appl. Catal. B: Environ.* **107**, p.p. 355– 362, 2011.

[10] Y. Huo, J. Zhang, M. Miao, Y. Jin. "Solvothermal synthesis of flower-like BiOBr microspheres with highly visible-light photocatalytic performances", *Appl. Catal. B: Environ.* **111-112**, pp. 334– 341, 2012.

[11] J. Xia, S. Yin, H. Li, H. Xu, L. Xu, Y. Xu. "Improved visible light photocatalytic activity of sphere-like BiOBr hollow and porous structures synthesized via a reactable ionic liquid", *Dalton Trans.*, **40**, pp. 5249, 2011.

[12] F. Yanfen, H. Yingping, Y. Jing, W. Pan, C. Genwei. "Unique Ability of BiOBr To Decarboxylate D-Glu and D-MeAsp in the Photocatalytic Degradation of Microcystin-LR in Water", *Environ. Sci. Technol.*, **45**, pp. 1593–1600, 2011.

[13] H. Deng, J. Wang, Q. Peng, X. Wang, Y. Li, "Controlled Hydrothermal Synthesis of Bismuth Oxyhalide Nanobelts and Nanotubes", *Chem. Eur. J.*, **11**, pp. 6519 –6524, 2005.

[15] C. Jovalekic, M. Pavlovic, P. Osmokrovic, L. Atanasoska. "X-ray photoelectron spectroscopy study of $Bi_4Ti_3O_{12}$ ferroelectric ceramics", *Appl. Phys. Lett.*, **72**, pp. 1051-1053, 1998.

[16] J. Zhang, F. Shi, J. Lin, D. Chen, J. Gao, Z. Huang, X. Ding, C. Tang. "Self-Assembled 3-D Architectures of BiOBr as a Visible Light-Driven Photocatalyst", *Chem. Mater.*, **20**, pp. 2937-2941, 2008.